PHOTONICS Research

# Universal dynamics and deterministic motion control of decoherently seeded temporal dissipative solitons via spectral filtering effect

Zilong Li,[1] Huanhuan Liu,[2,5] Zimin Zha,[1] Lei Su,[3] Perry Ping Shum,[4] and Hairun Guo[1,6]

[1]Key Laboratory of Specialty Fiber Optics and Optical Access Networks, Joint International Research Laboratory of Specialty Fiber Optics and Advanced Communication, Shanghai University, Shanghai 200044, China
[2]Shenzhen Institute of Advanced Technology, Chinese Academy of Sciences, Shenzhen 518055, China
[3]School of Engineering and Materials Science, Queen Mary University of London, London E1 4NS, UK
[4]Department of Electrical and Electronic Engineering, Southern University of Science and Technology, Shenzhen 518055, China
[5]e-mail: lhh_ly@163.com
[6]e-mail:hairun.guo@shu.edu.cn

Received 26 July 2023; revised 26 September 2023; accepted 26 September 2023; posted 27 September 2023 (Doc. ID 500126); published 22 November 2023

**Temporal dissipative solitons have been widely studied in optical systems, which exhibit various localized structures and rich dynamics, and have shown great potential in applications including optical encoding and sensing. Yet, most of the soliton states, as well as the switching dynamics amongst, were fractionally captured or via self-evolution of the system, lacking of control on the soliton motion. While soliton motion control has been widely investigated in coherently seeded optical cavities, such as microresonator-based dissipative solitons, its implementation in decoherently seeded systems, typically the soliton mode-locked lasers, remains an outstanding challenge. Here, we report the universal dynamics and deterministic motion control of temporal dissipative solitons in a mode-locked fibre laser by introducing a scanned spectral filtering effect. We investigate rich switching dynamics corresponding to both the assembly and the disassembly of solitons, revealing a complete and reversible motion from chaotic states to soliton and soliton-molecule states. Significant hysteresis has been recognized in between the redshift and blueshift scan of the motorized optical filter, unveiling the nature of having state bifurcations in dissipative and nonlinear systems. The active soliton motion control enabled by filter scanning highlights the potential prospects of encoding and sensing using soliton molecules.** 

https://doi.org/10.1364/PRJ.500126

## 1. INTRODUCTION

Temporal dissipative solitons result from the composite balance between nonlinearity and dispersion, gain and loss [1]. Compared with the case of conventional solitons, the impact of dissipative effects reveals unusual situations in which complex localized structures can be found, such as soliton breathers [2–5], and the coexistence of a large number of solitons (quadruple solitons [6], soliton crystals [7,8], and soliton molecules [9–13]). In general, dissipative solitons are basically generated from coherently seeded and decoherently seeded systems. In typical coherently seeded systems, such as microresonator-based solitons [14–17] or laser cavities with parametric gain [18–21], motion control of solitons can be directly realized by adjusting the seeding conditions.

For example, in a fibre ring resonator that supports the formation of temporal dissipative soliton driven by a localized continuous wave laser, deterministic writing and erasing of solitons are allowed via pump modulation [19]. Moreover it has been demonstrated that the thermal-optic effect in microresonators could cause non-degenerate states of different soliton number, and enable the access to each soliton state by simply backward wavelength tuning the pumping laser [14]. In addition all-optical switching between soliton molecule states with different binding separations could also be controlled by a parametric gain modulation in an optical oscillator [20].

However in contrast to coherently seeded systems, motion control remains challenging in laser systems that are decoherently seeded (e.g., the gain in the laser cavity is via stimulated emission of carriers and therefore has decoherent link to the seeding source). Most researches have focused on instant switching dynamics of soliton states within a short moment, such as soliton formation [22–28], soliton synthesis and dissociation [28–31], solitons internal motion [32–35], solitons collision [36,37], and soliton breathers [4]. Noise-mediated soliton motion [38,39]

seems also possible in laser systems, yet it is inherently stochastic. Most necessarily, active motion control in decoherently seeded systems, especially for mode-locked lasers, relies on the introduction of extra parameter-controlled elements [40–45]. Even though build-up and dissociation of dissipative soliton molecules could be theoretically and experimentally observed under different transmission functions of saturable absorbers, the switching took place stochastically [28]. In addition, in hundreds of temporal "reactors," created in parallel in an opto-acoustically mode-locked fibre laser, one can achieve on-demand synthesis and dissociation of soliton molecules [30,46]. However, at present, a complete set of dynamics of regarding soliton motion and the switching in between different states is still not observed.

Here, we report the observation of a complete set of dynamics of temporal dissipative solitons motion in a mode-locked fibre laser controlled by the spectral filtering effect (SFE). We present a detailed analysis of the observed phenomenon and demonstrate its universal nature. Single switching dynamics of soliton disassembly are observed at one moment when a single soliton is dissociated from a complex soliton molecule. We also observe complex switching dynamics of a soliton pair combined with a single soliton, including complicated soliton assembly and disassembly. Moreover, we investigate the complete soliton switching dynamics of filter scanning and record all dynamics at each switching moment, in which we observe a significant hysteresis between redshift and blueshift. From an application perspective, the presented results provide a new method for temporal dissipative solitons motion control in the decoherently seeded system.

## 2. RESULTS

The experimental setup is shown in Fig. 1(a). The focused decoherently seeded system is an erbium-doped mode-locked fibre laser using carbon-nanotube-based saturable absorber (CNT-SA). A 3.1-m length erbium-doped fibre (EDF, LIEKKI 30/4) is used as the gain medium, and the total length of the single-mode fibre (SMF) is ∼8.15 m. Thus, the corresponding basic repetition frequency of the cavity is ∼18.167 MHz. The net cavity dispersion at the wavelength of 1.56 μm is ∼ −0.135 $ps^2$. The function of the polarization controller in the laser cavity is to enhance the birefringence on the cavity mode and to enable the self-starting of the laser at a relative low pumping power, which has been widely applied [47,48]. Regarding our lasers, the threshold pumping power for reaching the mode-locking state could be as low as ∼23.71 mW, which is much lower compared with nonlinear polarization evolution lasers [33,34]. The output signals are detected by a 33 GHz photodetector (N7004A, Keysight) and recorded by a 59 GHz, 160 GSa/s real-time oscilloscope (DSAZ592A, Keysight).

As shown in Fig. 1(d), the bandwidth of a tuneable bandpass filter (TBPF) is ∼40 nm, and its centre wavelength is tuneable in the range of 1520–1600 nm. For the dispersion Fourier transform (DFT) based real-time spectrum system, a 5-km length dispersion compensation fibre (DCF) is used as the dispersion medium to provide a total cumulative dispersion of ∼ −679 ps/nm at 1545 nm. The duration of stretched pulse $\Delta\tau$ can be calculated by [34,49]

$$\Delta\tau = |\mathrm{DL}|\Delta\lambda, \tag{1}$$

in which $\Delta\lambda$ is the wavelength range of the input signal, and DL is total cumulative dispersion of dispersive medium. Therefore, the scale of wavelength to time mapping is ∼1.47 nm/ns. Meanwhile, the maximum time resolution of the detecting system is ∼0.1 ns; the corresponding maximum electronic spectral resolution is ∼0.147 nm. In addition, the maximum 3-dB bandwidth of soliton spectrum is ∼3.1 nm; the 30-dB bandwidth of that is ∼12.5 nm. Therefore, calculated temporal separation is 8.5 ns, meaning that pulses with a separation greater than 8.5 ns are recognized as two separate pulses in the time domain, while pulses that are closer would be transformed to reveal the spectral profile, cf. Figs. 5(e)–5(h) as an example.

While the centre wavelength of the TBPF is set at the centre wavelength of the laser output, all effective spectra are included in the pass band of TBPF. By carefully adjusting the TBPF, the red and blue boundaries of the filtered gain spectrum can be determined. Beyond the boundaries, the intracavity gain fibre cannot provide enough gain to form temporal solitons. During long-term filtering scanning, the temporal dynamic evolution of intracavity solitons is shown in an oscilloscope (OSC), such as the evolution of two-soliton molecules (TSMs) into complex soliton molecules (CSMs), as shown in Figs. 1(c) and 1(f). Due to the limitation of oscilloscope resolution, the directly recorded pulse trains cannot distinguish the fine structure of soliton molecules. Therefore, a power stage of pulse trains is clearly shown in OSC. Figure 1(e) shows a typical spectrum of solitons that are affected by the edge of the bandpass filter, which reveals a similar edge on the spectral profile.

In order to directly observe the switching dynamics of solitons, the soliton spectra of each roundtrip are mapped to the pulse train in time domain via DFT, and the switching moment of solitons could be recorded by an oscilloscope. In our work, two methods were used to assist quickly and accurately the collection of the split-second switching moments. On the one hand, the original signal is set as a trigger signal, and some switching moments with distinct power stage can be precisely collected by setting an appropriate trigger level. On the other hand, the external burst signal is alternative as the trigger; further, all switching moments can be recorded by setting an appropriate time delay, as shown in Fig. 1(c).

### A. Single Switching Dynamics

The gain spectrum of the fibre cavity is jointly determined by the gain fibre and TBPF. The gain fibre is uniquely determined, and the intracavity gain changes accordingly when the TBPF is tuned. The composite balance between gain and loss, nonlinearity and dispersion is re-established and expresses different soliton states. The real-time responses to this effect are the relative motion of solitons and change of soliton characteristics, such as intensity, phase, and separation.

The experiments reveal a relationship between SFE and the soliton switching. When the centre wavelength of TBPF is ∼1568 nm and the centre wavelength is continuously tuned, one moment of deterministic switching is recorded via DFT. Figure 2 shows the switching dynamics between CSM and TSM, specifically, solitons disassembly. The complete

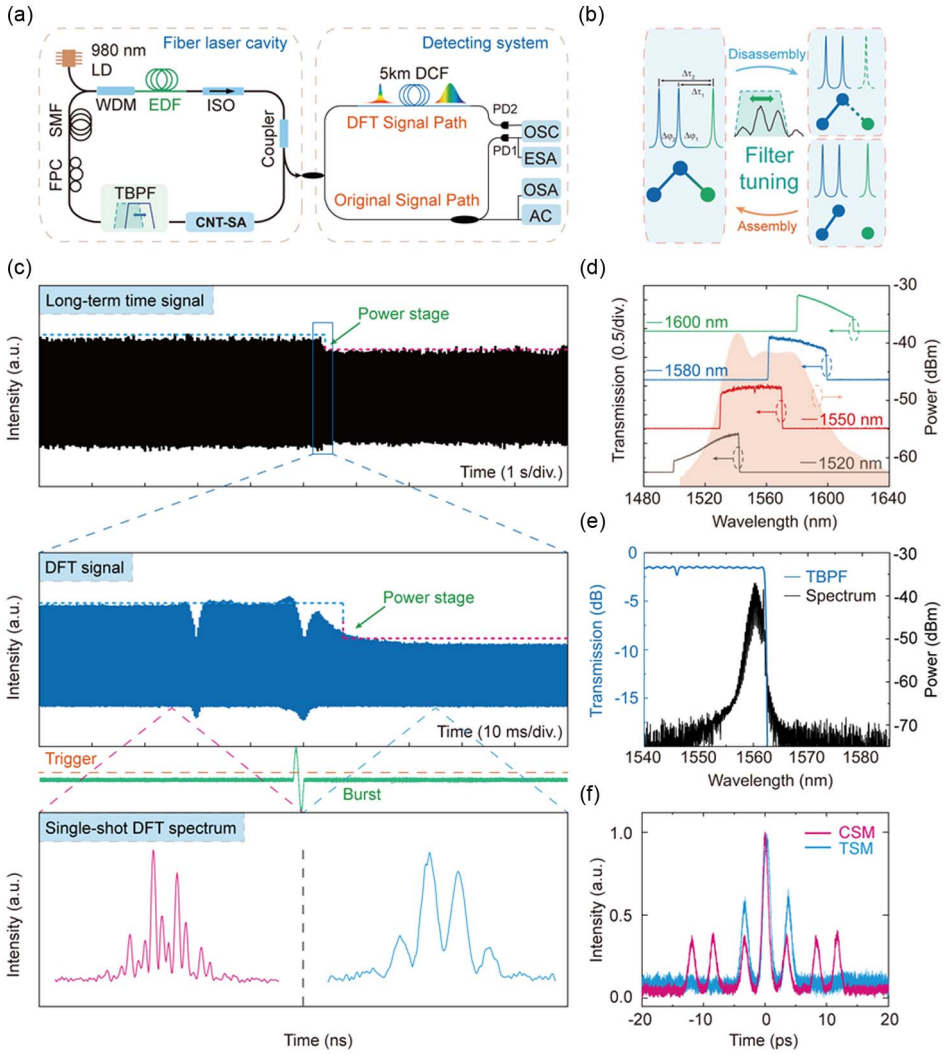


**Fig. 1.** Motion control of decoherently seeded temporal dissipative solitons via SFE. (a) Sketch of the experimental setup, including an erbium-doped mode-locked fibre laser (mode locking is under the pump power of ~23.71 mW) incorporating a carbon-nanotube-based saturable absorber (CNT-SA) and real-time spectrum measurement system based on DFT method. LD, laser diode; SMF, single-mode fibre; EDF, erbium-doped fibre; WDM, wavelength-division multiplexer; FPC, fibre polarization controller; ISO, isolator; TBPF, tuneable bandpass filter; DCF, dispersion compensation fibre; OSA, optical spectrum analyzer; AC, autocorrelator; ESA, electrical spectrum analyzer; OSC, oscilloscope; PD, photodetector. (b) Conceptual illustration of temporal dissipative solitons assembly and disassembly via SFE. (c) Data acquisition technology route. (d) Transmission of TBPF; the shaded part is the amplified spontaneous emission spectrum of EDF. (e) Transmission spectrum of TBPF with sharp edges and the output spectrum of fibre laser (the centre wavelength of TBPF is ~1543 nm). (f) Autocorrelation traces of two-soliton molecules (TSMs) and complex soliton molecules (CSMs).

transition from a CSM state to a TSM state is illustrated in Fig. 2(c), while Fig. 2(e) shows significant details at the beginning of the transition. From Figs. 2(e) and 2(f), one could conclude that the transition is via the dissembling of one pulse from the CSM, where the temporal separation between the pulse and the molecule is increased, accompanied with an accumulative change in the phase. Moreover, limited by the resolution of the retrieved spectrum, the evaluated autocorrelation trace is within a time range of ~55.4 ps. Hence, there may have a folding effect [Fig. 2(d)] when the free pulse is separate far away outside the effective range. In practice, we unfolded the evolution of the autocorrelation trace and retrieve a complete dissembling dynamic during the CSM to TSM transition.

### B. Complex Switching Dynamics

We next observe the complex switching dynamics of solitons assembly at a second moment. When the centre wavelength of TBPF is ~1555 nm and continuously tuned, we first have stable TSMs circulating in the cavity and subsequently switch to CSMs, as shown in Figs. 3(a) and 3(b). The transition also features self-adjustment on the interval in between solitons, once the CSM state is formed (corresponding to the roundtrips 107,000–120,000).

Figure 3(c) shows nine slices within the whole transition, revealing detailed soliton motions. Solitons do not simply approach each other directly but go through a complex intermediate process. This is largely similar to the formation of intermediate products in chemical reactions of substance

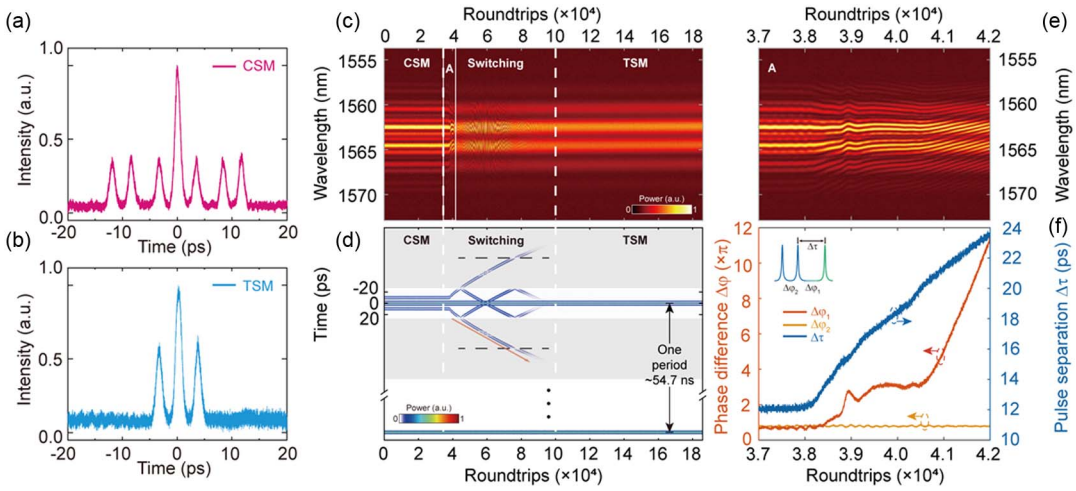


**Fig. 2.** One moment single switching dynamics of solitons disassembly. Autocorrelation traces of (a) CSM and (b) TSM. (c) Spectral evolution dynamics of soliton disassembly. (d) Autocorrelation trace evolution dynamics of soliton disassembly. (e) Enlarged view of area A in (c). Disassembly of the soliton begins to occur. (f) Evolution of phase differences and separations between the soliton of soliton pairs and single soliton, corresponding to 5000 roundtrips in (e). (CSM to TSM, the centre wavelength of TBPF is ∼1568 nm.)

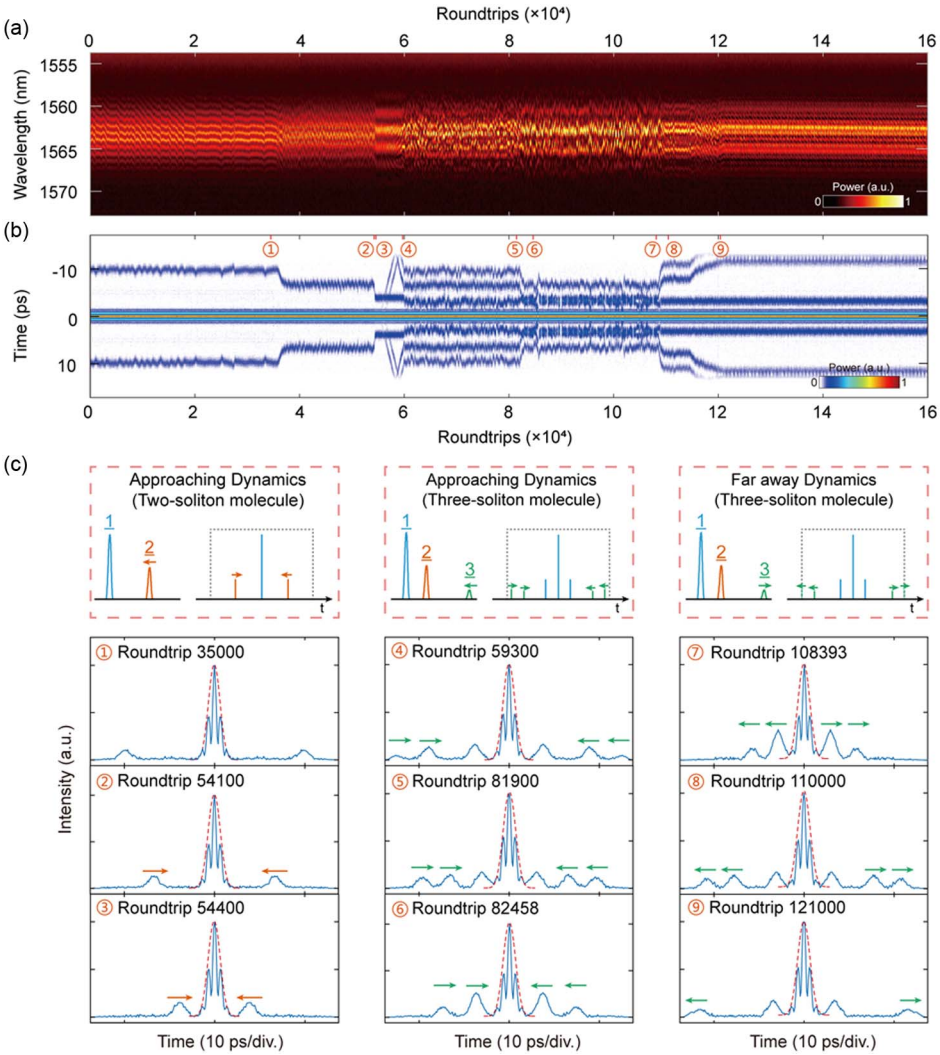


**Fig. 3.** One moment complex switching dynamics of solitons assembly. (a) Real-time spectra and (b) autocorrelation traces. (c) Dynamic decomposition of soliton assembly. Dashed line represents the main peak of the filtered autocorrelation trace. In particular, soliton No. 3 moves out of the temporal boundary observed by the detecting system during soliton far away. (TSM to CSM, the centre wavelength of TBPF is ∼1555 nm.)

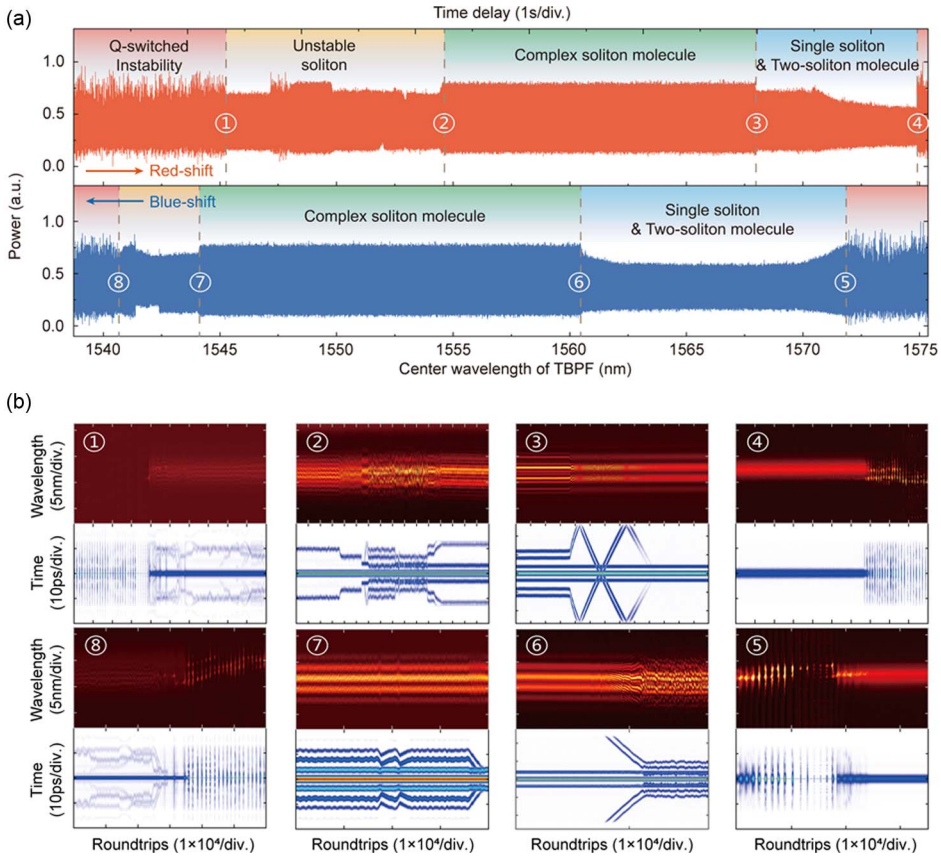


**Fig. 4.** Full switching dynamics of motion control. (a) Long-term switching dynamics of temporal dissipative solitons during TBPF scanning, including redshift and blueshift. The scanning speed is ∼4.89 nm/s. (b) Real time spectra at the switching moments, corresponding to pulse state switching in time domain (a). Panels 1 and 8: switching between $Q$-switching instability and unstable soliton in redshift and blueshift, respectively; panels 2, 3, 6, and 7, switching between a two-soliton molecule and complex soliton molecule in redshift and blueshift, respectively; panels 4 and 5, switching between single soliton and $Q$-switching instability in redshift and blueshift, respectively.

molecules. The CSMs with a mutative interval between single soliton and soliton pair are intermediate products of this complex switching. The bonds between solitons undergo complex processes such as multiple breaks and recombination; subsequently, solitons recombine into new soliton molecules.

### C. Full Switching Dynamics

We recorded the full switching dynamics of temporal dissipative solitons via filter scanning. The TBPF is controlled by a programable motor to scan in the redshift and blueshift directions. At the moment, the tuning of the bandpass filter is at a speed of ∼4.89 nm/s. In the meantime, the spectral resolution of the DFT system is ∼0.147 nm. In this way, tuning the filter to have a resolvable change in the wavelength may take ∼30 ms, which is more than 100 times longer compared with the build-up time (∼100 μs) of the mode-locked laser [23]. Therefore, the scan of the filter is relatively in the static mode. The filter scanning is operated starting from different states, such as two-soliton molecules and complex soliton molecules (see Visualization 1 and Visualization 2). The whole tuning process starting from complex soliton molecules includes complete soliton states, such as $Q$-switched instability, unstable soliton, complex soliton molecule, two-soliton molecule, and single soliton, as shown in Fig. 4(a). More obviously, the blueshift process shows significant hysteresis in contrast with the redshift process, which is a typical characteristic of the mode-locked fibre laser, a nonlinear optical system.

As shown in Fig. 4(b), combined with two data acquisition methods, we collected all switching dynamics at each moment. When the TBPF is near the boundary, the net gain of the cavity is greatly limited and cannot accumulate enough energy to form solitons. Thus, the laser is under the $Q$-switched instability state of kHz repetition rate. With the redshift of TBPF, the net gain window gradually becomes larger, and the laser begins to form unstable solitons, cf. the state 1 in Fig. 4(b), and state 8 during the blueshift scan of the filter. When the net gain window is fully open, solitons undergo a complex intermediate process to form CSMs composed of the largest number of solitons (here are three solitons), as shown in Fig. 4(b) panel 2, which corresponds to Fig. 4(b) panel 7 during the blueshift. The filtering edge on the other side limits the net gain window as continuous scanning of TBPF, which results in solitons disassembly with single switching dynamics, as shown in Fig. 4(b) panel 3, which corresponds to Fig. 4(b) panel 6 during the blueshift. When approaching the right-hand boundary, two-soliton molecules first transform into a single soliton and then transform into $Q$-switching instability due to the narrowest net gain window in the red shift process, as shown in Fig. 4(b) panel 4, which corresponds to Fig. 4(b) panel 5 during the blueshift.

Such deterministic events, soliton assembly and disassembly, are not easy to occur in a dissipative system. However, it is still possible that a soliton interaction mechanism mediated by the continuum noise floor can lead to soliton drift in mode-locked fibre lasers [38,39]. Physically, the sharp edge on the soliton spectrum corresponds to an oscillating waveform in the time domain. This is understood as the main cause of soliton splitting and the cause for the formation of soliton molecules, provided that the effective gain in the laser cavity is also reduced by the filter. More importantly, by tuning the bandpass filter, such a responded oscillating wave is also travelling within the cavity, potentially resulting in the assembling and dissembling behaviors of the soliton molecule.

## 3. CONCLUSION

In conclusion, we have demonstrated universal dynamics and deterministic motion control of temporal dissipative solitons in a mode-locked fibre laser via the SFE. By introducing external element, TBPF, we could actively control the solitons motion for assembly and disassembly. This provides a deterministic route toward soliton switching inside decoherently seeded systems. Based on the DFT detecting system, we also investigated the completed dynamics at each moment. We observed specific dynamics of soliton assembly and disassembly and revealed the single and complex relative motion of solitons, which is like a chemical reaction of material molecules. These switches are the result of the SFE breaking the established balance of the laser cavity and rebuilding a new one.

## APPENDIX A: MEASUREMENT RANGE OF THE DFT-BASED DETECTING SYSTEM

In experiments, based on the DFT-based real-time spectrum measurement system, we measured the 10,000 roundtrips

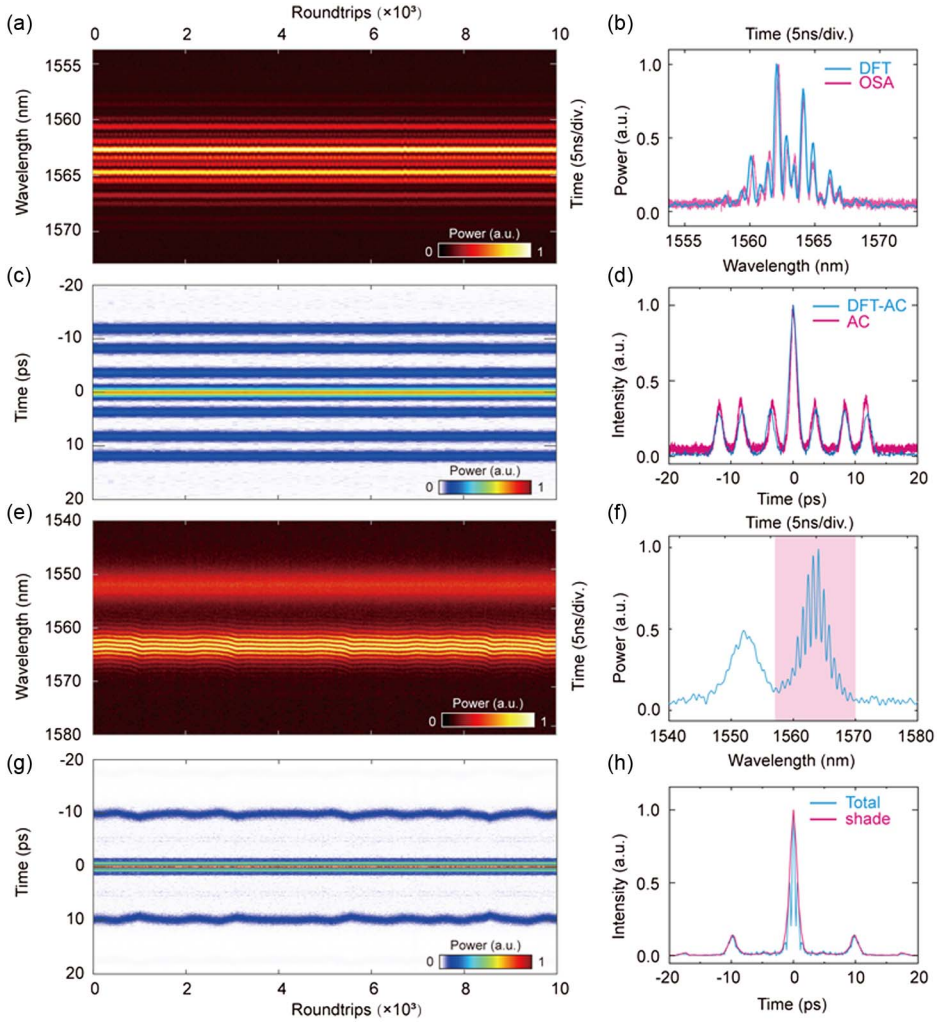


**Fig. 5.** Dynamics of stable temporal soliton molecules. 2D contour plots of 10,000 roundtrips consecutive single-shot spectrum (spectral intensity in colour scale) of (a) stable complex soliton molecule and (e) two-soliton molecule adjoined single pulse. Optical spectrum of (b) stable complex soliton molecule and (f) two-soliton molecule adjoined single pulse, as directly recorded by the OSA (red curves) and as the single-shot spectrum (in blue). Evolution of the intensity of the Fourier transforms of single-shot spectrum, namely, first-order single-shot autocorrelation traces (intensity in color scale) of (c) stable complex soliton molecule and (g) two-soliton molecule adjoined single pulse. (d) Autocorrelation trace, as directly recorded by the autocorrelator (red curves), and as the first-order single-shot autocorrelation traces (in blue) of stable complex soliton molecule. (h) First-order single-shot autocorrelation trace of two-soliton molecule adjoined single pulse before (in blue) and after (in red) filtering shadow region.

DFT spectrum of different soliton states and calculated the corresponding autocorrelation trace by Fourier transform, as shown in Fig. 5. Figures 5(a)–5(d) show the results of stable (1 + 2) complex soliton molecules. The comparison of a single-shot DFT spectrum and autocorrelation trace is shown in Figs. 5(b) and 5(d) with the average spectrum and autocorrelation trace measured simultaneously by an OSA and an autocorrelator. The spectra and autocorrelation traces reveal two matched spectra and time intervals. The modulation periods of 2.1 and 0.98 nm in the spectrum correspond to the 3.7 ps time interval in the molecule of a soliton pair and the 8.2 ps time interval between a soliton pair and single soliton.

In addition, in the experiment, we also recorded a special set of DFT signals, as shown in Figs. 5(e)–5(h). It is caused by the multipulse output state of the laser, and one of the pulse intervals exceeds the measurement effective range of the DFT measurement system. Therefore, the signal recorded in Fig. 5(f) is the superposition of the spectral signal in the shadow area and the adjacent time domain pulse signal, and there is obvious modulation on the crest of the corresponding autocorrelation trace. When we only calculate the DFT spectral signal in the shadow area by Fourier transform, the obtained autocorrelation trace is as shown in the red curve in Fig. 5(h), which represents the autocorrelation trace of the two-soliton molecule within the effective range of the measurement system.

## APPENDIX B: COUNTING SOLITON STATES UNDER MULTIPLE REPEATED EXPERIMENTS OF LONG-TERM FILTER SCANNING

In order to avoid experimental occasionality, the same experimental operations are repeated eight times. Specifically, back-and-forth filter scanning is performed starting from the same initial state (complex soliton molecule). We counted the number of occurrences of each soliton state in the measurement results, as shown in the Fig. 6. All soliton states are repeated accurately during the redshift process, while the state of complex soliton molecules is lost many times during the blue-shift process.

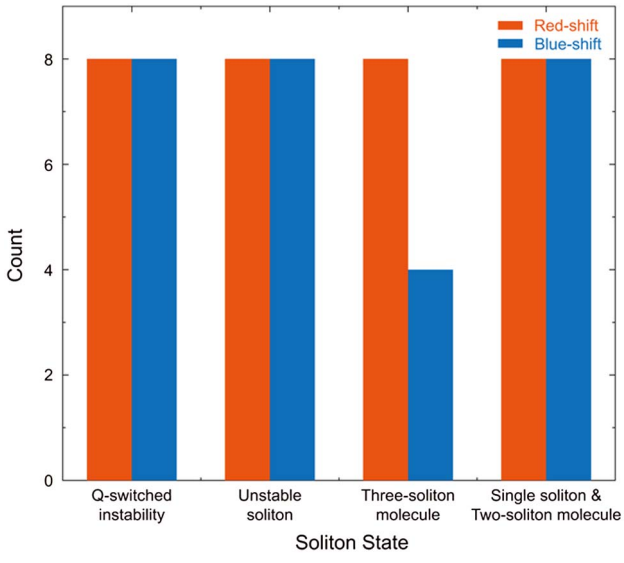


**Fig. 6.** Cartogram of soliton states under multiple repeated experiments of long-term filter scanning.

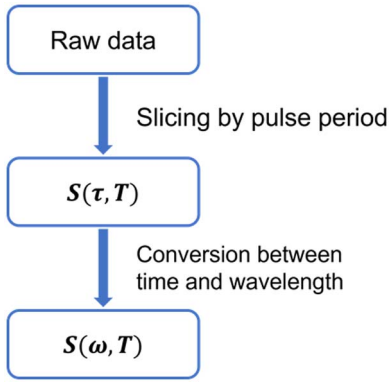


**Fig. 7.** Data processing route.

## APPENDIX C: DATA PROCESSING ROUTE

All data were processed using MATLAB. The raw data are usually huge, more than 2 GB. Figure 7 shows the data processing route. At first, the data for each roundtrip $S(\tau, T)$ are obtained by slicing the raw data by a pulse period in which $T$ is the slow time and $\tau$ is the fast time. Then, the fast time $\tau$ axis is converted to wavelength $\omega$, according to Eq. (1). The data for each roundtrip are spectrum $S(\omega, T)$. The corresponding autocorrelation trace can be obtained by doing a Fourier transform on the spectrum of each roundtrip. The final step is to perform arrangement of the processed data to obtain the 3D spectral evolution dynamics presented in figures.

Indeed, this method requires high performance of the oscilloscope. Alternatively, a strong coherent external trigger signal with the same repetition frequency of the fibre laser would reduce the requirements on the oscilloscope. By triggering the repetition frequency signal, the segmented memory acquisition of the oscilloscope could quickly acquire data of each period.

We illustrate the internal phase difference in the case of a TSM. The principle can be extended to molecules containing more solitons. The TSM is assumed to consist of two solitons of identical shape and amplitude, which have relative time intervals $\Delta\tau$ and phases $\Delta\varphi$. The electric field envelope of two-soliton molecule can be described by [22]

$$E(t) = \mathrm{Re}\{[E_1(t) + E_2(t)]\exp(i\omega_0 t)\}, \quad \textbf{(C1)}$$

where $E_2(t) = E_1(t + \Delta\tau)\exp(i\Delta\varphi)$. In the frequency domain, the TSM has the following spectral intensity:

$$S(\omega) = |E_1(\omega - \omega_0)|^2[1 + \cos(\omega\Delta\tau - \omega_0\Delta\tau + \Delta\varphi)], \quad \textbf{(C2)}$$

where $|E_1(\omega - \omega_0)|^2$ represents the envelope of the optical spectrum. Relative phase differences and time intervals can be obtained by fitting the spectra for each cycle based on Eq. (C2).

**Funding.** 111 Project (D20031); Science, Technology and Innovation Commission of Shenzhen Municipality (JCYJ20220530113811026); Shanghai Science and

Technology Development Foundation (20QA1403500); Natural Science Foundation of Guangdong Province (2022A1515011434); National Natural Science Foundation of China (11974234).

**Disclosures.** The authors declare no conflicts of interest.

**Data Availability.** Data underlying the results presented in this paper are not publicly available at this time but may be obtained from the authors upon reasonable request.

## REFERENCES


1. G. P. Agrawal, "Nonlinear fiber optics," in *Nonlinear Science at the Dawn of the 21st Century*, P. L. Christiansen, M. P. Sørensen, and A. C. Scott, eds. (Springer, 2000), pp. 195–211.
2. E. Lucas, M. Karpov, H. Guo, M. L. Gorodetsky, and T. J. Kippenberg, "Breathing dissipative solitons in optical microresonators," Nat. Commun. **8**, 736 (2017).
3. W. Chen, B. Garbin, A. U. Nielsen, S. Coen, S. G. Murdoch, and M. Erkintalo, "Experimental observations of breathing Kerr temporal cavity solitons at large detunings," Opt. Lett. **43**, 3674–3677 (2018).
4. J. Peng, S. Boscolo, Z. Zhao, and H. Zeng, "Breathing dissipative solitons in mode-locked fiber lasers," Sci. Adv. **5**, eaax1110 (2019).
5. J. Peng, Z. Zhao, S. Boscolo, C. Finot, S. Sugavanam, D. V. Churkin, and H. Zeng, "Breather molecular complexes in a passively mode-locked fiber laser," Laser Photon. Rev. **15**, 2000132 (2021).
6. W. He, M. Pang, D. H. Yeh, J. Huang, C. R. Menyuk, and P. St.J. Russell, "Formation of optical supramolecular structures in a fibre laser by tailoring long-range soliton interactions," Nat. Commun. **10**, 5756 (2019).
7. D. C. Cole, E. S. Lamb, P. Del'Haye, S. A. Diddams, and S. B. Papp, "Soliton crystals in Kerr resonators," Nat. Photonics **11**, 671–676 (2017).
8. Z. Lu, H.-J. Chen, W. Wang, L. Yao, Y. Wang, Y. Yu, B. E. Little, S. T. Chu, Q. Gong, W. Zhao, X. Yi, Y.-F. Xiao, and W. Zhang, "Synthesized soliton crystals," Nat. Commun. **12**, 3179 (2021).
9. P. Grelu and N. Akhmediev, "Dissipative solitons for mode-locked lasers," Nat. Photonics **6**, 84–92 (2012).
10. Y. Y. Luo, R. Xia, P. P. Shum, W. J. Ni, Y. Liu, H. Q. Lam, Q. Sun, X. H. Tang, and L. M. Zhao, "Real-time dynamics of soliton triplets in fiber lasers," Photon. Res. **8**, 884–891 (2020).
11. S. Hamdi, A. Coillet, B. Cluzel, P. Grelu, and P. Colman, "Superlocalization reveals long-range synchronization of vibrating soliton molecules," Phys. Rev. Lett. **128**, 213902 (2022).
12. X. Hu, J. Guo, J. Wang, J. Ma, L. Zhao, S. Yoo, and D. Tang, "Novel optical soliton molecules formed in a fiber laser with near-zero net cavity dispersion," Light Sci. Appl. **12**, 38 (2023).
13. S. Huang, Y. Liu, H. Liu, Y. Sun, R. Xia, W. Ni, Y. Luo, L. Yan, H. Liu, Q. Sun, P. P. Shum, and X. Tang, "Isomeric dynamics of multi-soliton molecules in passively mode-locked fiber lasers," APL Photon. **8**, 036105 (2023).
14. H. Guo, M. Karpov, E. Lucas, A. Kordts, M. H. P. Pfeiffer, V. Brasch, G. Lihachev, V. E. Lobanov, M. L. Gorodetsky, and T. J. Kippenberg, "Universal dynamics and deterministic switching of dissipative Kerr solitons in optical microresonators," Nat. Phys. **13**, 94–102 (2017).
15. T. Huang, J. Pan, Z. Cheng, G. Xu, Z. Wu, T. Du, S. Zeng, and P. P. Shum, "Nonlinear-mode-coupling-induced soliton crystal dynamics in optical microresonators," Phys. Rev. A **103**, 023502 (2021).
16. A. Völkel, L. Nimmesgern, A. Mielnik-Pyszczorski, T. Wirth, and G. Herink, "Intracavity Raman scattering couples soliton molecules with terahertz phonons," Nat. Commun. **13**, 2066 (2022).
17. G. Xu, A. U. Nielsen, B. Garbin, L. Hill, G.-L. Oppo, J. Fatome, S. G. Murdoch, S. Coen, and M. Erkintalo, "Spontaneous symmetry breaking of dissipative optical solitons in a two-component Kerr resonator," Nat. Commun. **12**, 4023 (2021).
18. G. Herink, B. Jalali, C. Ropers, and D. R. Solli, "Resolving the build-up of femtosecond mode-locking with single-shot spectroscopy at 90 MHz frame rate," Nat. Photonics **10**, 321–326 (2016).
19. I. Hendry, B. Garbin, S. G. Murdoch, S. Coen, and M. Erkintalo, "Impact of desynchronization and drift on soliton-based Kerr frequency combs in the presence of pulsed driving fields," Phys. Rev. A **100**, 023829 (2019).
20. F. Kurtz, C. Ropers, and G. Herink, "Resonant excitation and all-optical switching of femtosecond soliton molecules," Nat. Photonics **14**, 9–13 (2020).
21. Y. Wang, F. Leo, J. Fatome, M. Erkintalo, S. G. Murdoch, and S. Coen, "Universal mechanism for the binding of temporal cavity solitons," Optica **4**, 855–863 (2017).
22. G. Herink, F. Kurtz, B. Jalali, D. R. Solli, and C. Ropers, "Real-time spectral interferometry probes the internal dynamics of femtosecond soliton molecules," Science **356**, 50–54 (2017).
23. X. Liu, X. Yao, and Y. Cui, "Real-time observation of the buildup of soliton molecules," Phys. Rev. Lett. **121**, 023905 (2018).
24. J. S. Peng, M. Sorokina, S. Sugavanam, N. Tarasov, D. V. Churkin, S. K. Turitsyn, and H. P. Zeng, "Real-time observation of dissipative soliton formation in nonlinear polarization rotation mode-locked fibre lasers," Commun. Phys. **1**, 20 (2018).
25. J. S. Peng and H. P. Zeng, "Build-up of dissipative optical soliton molecules via diverse soliton interactions," Laser Photon. Rev. **12**, 1800009 (2018).
26. S. Sun, Z. Lin, W. Li, N. Zhu, and M. Li, "Time-stretch probing of ultrafast soliton dynamics related to *Q*-switched instabilities in mode-locked fiber laser," Opt. Express **26**, 20888–20901 (2018).
27. X. Liu and M. Pang, "Revealing the buildup dynamics of harmonic mode-locking states in ultrafast lasers," Laser Photon. Rev. **13**, 1800333 (2019).
28. Y. Zhou, Y.-X. Ren, J. Shi, H. Mao, and K. K. Y. Wong, "Buildup and dissociation dynamics of dissipative optical soliton molecules," Optica **7**, 965–972 (2020).
29. J. S. Peng and H. P. Zeng, "Dynamics of soliton molecules in a normal-dispersion fiber laser," Opt. Lett. **44**, 2899–2902 (2019).
30. W. He, M. Pang, D.-H. Yeh, J. Huang, and P. St.J. Russell, "Synthesis and dissociation of soliton molecules in parallel optical-soliton reactors," Light Sci. Appl. **10**, 120 (2021).
31. Y. Du, Z. He, Q. Gao, C. Zeng, D. Mao, and J. Zhao, "Intermediate state between a solitary singlet and a molecule in lasers," Phys. Rev. A **107**, 053512 (2023).
32. J. Igbonacho, K. Nithyanandan, K. Krupa, P. T. Dinda, P. Grelu, and A. B. Moubissi, "Dynamics of distorted and undistorted soliton molecules in a mode-locked fiber laser," Phys. Rev. A **99**, 063824 (2019).
33. K. Krupa, K. Nithyanandan, U. Andral, P. Tchofo-Dinda, and P. Grelu, "Real-time observation of internal motion within ultrafast dissipative optical soliton molecules," Phys. Rev. Lett. **118**, 243901 (2017).
34. Z. Q. Wang, K. Nithyanandan, A. Coillet, P. Tchofo-Dinda, and P. Grelu, "Optical soliton molecular complexes in a passively mode-locked fibre laser," Nat. Commun. **10**, 830 (2019).
35. A. U. Nielsen, Y. Xu, C. Todd, M. Ferré, M. G. Clerc, S. Coen, S. G. Murdoch, and M. Erkintalo, "Nonlinear localization of dissipative modulation instability," Phys. Rev. Lett. **127**, 123901 (2021).
36. Y. Wei, B. Li, X. Wei, Y. Yu, and K. K. Y. Wong, "Ultrafast spectral dynamics of dual-color-soliton intracavity collision in a mode-locked fiber laser," Appl. Phys. Lett. **112**, 081104 (2018).
37. H. Liang, X. Zhao, B. Liu, J. Yu, Y. Liu, R. He, J. He, H. Li, and Z. Wang, "Real-time dynamics of soliton collision in a bound-state soliton fiber laser," Nanophotonics **9**, 1921–1929 (2020).
38. R. Weill, A. Bekker, V. Smulakovsky, B. Fischer, and O. Gat, "Noise-mediated Casimir-like pulse interaction mechanism in lasers," Optica **3**, 189–192 (2016).
39. K. Sulimany, O. Lib, G. Masri, A. Klein, M. Fridman, P. Grelu, O. Gat, and H. Steinberg, "Bidirectional soliton rain dynamics induced by Casimir-like interactions in a graphene mode-locked fiber laser," Phys. Rev. Lett. **121**, 133902 (2018).
40. L. Nimmesgern, C. Beckh, H. Kempf, A. Leitenstorfer, and G. Herink, "Soliton molecules in femtosecond fiber lasers: universal binding mechanism and direct electronic control," Optica **8**, 1334–1339 (2021).

41. Y. Zhou, J. Shi, Y.-X. Ren, and K. K. Y. Wong, "Reconfigurable dynamics of optical soliton molecular complexes in an ultrafast thulium fiber laser," Commun. Phys. **5**, 302 (2022).
42. Y. Zhang, X. Tian, Y. Duan, S. Liu, Z. Ding, and C. Tan, "Coherent control of optical soliton interaction via electromagnetically induced transparency with spatial modulation," AIP Adv. **11**, 125118 (2021).
43. Y. Zhou, Y.-X. Ren, J. Shi, and K. K. Y. Wong, "Breathing dissipative soliton molecule switching in a bidirectional mode-locked fiber laser," Adv. Photon. Res. **3**, 2100318 (2022).
44. Y. Liu, S. Huang, Z. Li, H. Liu, Y. Sun, R. Xia, L. Yan, Y. Luo, H. Liu, G. Xu, Q. Sun, X. Tang, and P. P. Shum, "Phase-tailored assembly and encoding of dissipative soliton molecules," Light Sci. Appl. **12**, 123 (2023).
45. Y. Song, D. Zou, O. Gat, M. Hu, and P. Grelu, "Chaotic internal dynamics of dissipative optical soliton molecules," Laser Photon. Rev. **17**, 2300066 (2023).
46. S. Liu, Y. Cui, E. Karimi, and B. A. Malomed, "On-demand harnessing of photonic soliton molecules," Optica **9**, 240–250 (2022).
47. Q. Bao, H. Zhang, Y. Wang, Z. Ni, Y. Yan, Z. X. Shen, K. P. Loh, and D. Y. Tang, "Atomic-layer graphene as a saturable absorber for ultrafast pulsed lasers," Adv. Funct. Mater. **19**, 3077–3083 (2009).
48. H. Zhang, D. Tang, R. J. Knize, L. Zhao, Q. Bao, and K. P. Loh, "Graphene mode locked, wavelength-tunable, dissipative soliton fiber laser," Appl. Phys. Lett. **96**, 111112 (2010).
49. K. Goda and B. Jalali, "Dispersive Fourier transformation for fast continuous single-shot measurements," Nat. Photonics **7**, 102–112 (2013).